ACS APPLIED MATERIALS & INTERFACES

Research Article

www.acsami.org

Thin MoS_2 Nanoflakes Encapsulated in Carbon Nanofibers as High-Performance Anodes for Lithium-Ion Batteries

Chenyang Zhao,[†] Junhua Kong,[‡] Xiayin Yao,[†] Xiaosheng Tang,[‡] Yuliang Dong,[†] Si Lei Phua,[†] and Xuehong Lu*[,†,‡]

[†]School of Materials Science and Engineering, Nanyang Technological University, 50 Nanyang Avenue, Singapore 639798

[‡]Temasek Laboratories @ NTU, Nanyang Technological University, 9th Storey, BorderX Block, Research Techno Plaza, 50 Nanyang Drive, Singapore 637553

Supporting Information

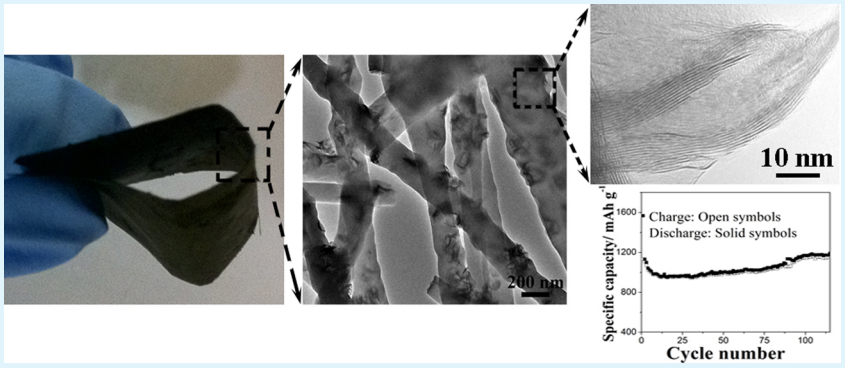

ABSTRACT: In this work, highly flexible MoS_2-based lithium-ion battery anodes composed of disordered thin MoS_2 nanoflakes encapsulated in amorphous carbon nanofibrous mats were fabricated for the first time through hydrothermal synthesis of graphene-like MoS_2, followed by electrospinning and carbonization. X-ray diffraction as well as scanning and transmission electron microscopic studies show that the as-synthesized MoS_2 nanoflakes have a thickness of about 5 nm with an expanded interlayer spacing, and their structure and morphology are well-retained after the electrospinning and carbonization. At relatively low MoS_2 contents, the nanoflakes are dispersed and well-embedded in the carbon nanofibers. Consequently, excellent electrochemical performance, including good cyclability and high rate capacity, was achieved with the hybrid nanofibrous mat at the MoS_2 content of 47%, which may be attributed to the fine thickness and multilayered structure of the MoS_2 sheets with an expanded interlayer spacing, the good charge conduction provided by the high-aspect-ratio carbon nanofibers, and the robustness of the nanofibrous mat.

KEYWORDS: *molybdenum disulfide (MoS_2), hydrothermal, electrospinning, carbon nanofibers, lithium-ion battery, flexible anode*

INTRODUCTION

In recent years, lithium-ion batteries (LIBs) have received greatly increased attention from both the academic and the industrial world because of their high energy density, low gravimetric density, long cycle life, and flexible design.[1] The commercial LIB anode material, graphite, has, however, a theoretical specific capacity of only 372 mAh/g,[2] which is too low to meet the rising demands for some emerging applications, such as electric vehicles. Recently, intensive research on graphene has spurred great interests in two-dimensional transition-metal dichalcogenides MX_2 (M = Ti, Nb, Mo, Ta; X = S, Se, Te) because they are promising alternatives for LIB anode materials. As an analogue of graphene, MX_2 has a layered structure, in which covalent bonds predominate within the layer, while van der Waals forces are regnant between the layers. The weak interlayer interaction allows the intercalation of foreign species into the layer, providing the possibility to achieve single-layered MX_2 and multilayered MX_2 with disordered structures.[3] Such MX_2 nanostructures have a large specific surface area, short diffusion length in the thickness direction, as well as abundant voids and defects that may benefit lithiation/delithiation.[4−6]

Among different types of MX_2, molybdenum disulfide (MoS_2) is the most stable and versatile member that exhibits the highest Li^+ ion capacity.[7−11] So far, various multilayered MoS_2 nanostructures, such as nanowires and nanotubes,[12] nanoflowers,[13] nanosheets,[14] and nanoflakes,[15] have been synthesized and applied as cathodes and anodes for LIBs.[16−19] However, these MoS_2-based anodes suffer from rapid capacity fading due to structure destruction induced by their large volume change in cycling. A possible way to solve this problem is to fabricate hybrid nanostructures.[20−23] Chen et

Received: December 17, 2013
Accepted: April 4, 2014
Published: April 4, 2014

   dx.doi.org/10.1021/am4058088 | ACS Appl. Mater. Interfaces 2014, 6, 6392−6398

al. synthesized graphene-like MoS_2/amorphous carbon composites by a hydrothermal route and found that the cycling stability of the composites was greatly enhanced owing to the enhanced conductivity and mechanical buffering effect of carbon.[24,25] Lemmon et al. prepared MoS_2/polyethylene (PEO) composites, and the incorporation of PEO stabilized the disordered structure of MoS_2 throughout the cycling regime.[26,27] Another route is to enlarge the interlayer distance of MoS_2, which will also introduce voids and defects into MoS_2 to improve its Li^+ ion storage capacity.[28,29] For instance, Guo et al. reported that restacked MoS_2 with an enlarged interlayer distance could exhibit superior stability and higher reversible capacity than the raw material.[30] Cho et al. reported that disordered MoS_2 nanoplates with an interlayer distance of 0.69 nm could exhibit excellent rate capability even at 53.1 A/g.[31] These research findings indicate that the high performance of MoS_2-based anodes is rooted in the relief of the stress induced by cycling to maintain the structural stability.

Electrospinning, a powerful technique for mass production of nanofibers, is an attractive approach for large-scale fabrication of MoS_2/carbon (MoS_2/C) hybrid nanofibers. The features of electrospun nanofibers, such as high aspect ratio and large surface area, may render the obtained hybrids good electrochemical properties,[1,32−35] while the carbon may effectively accommodate the volume change of MoS_2 in cycling. The obtained binder-free self-standing nanofibrous mats can be directly used as an anode after simply punching the mats into a suitable size and shape. Furthermore, since thin MoS_2 nanosheets are flexible, similar to that of multilayer graphene, when they are dispersed in carbon nanofibers, excellent flexibility of the structure may be achieved, enabling realization of diverse flexible LIBs.[36] In this work, we prepared the free-standing MoS_2/carbon nanofibrous mats via electrospinning and carbonization for the first time. In this article, the electrochemical properties of the MoS_2/C hybrid mats are reported and correlated to their morphology and structure. The mechanism for the good performance of the MoS_2/C anode is also clarified.

EXPERIMENTAL SECTION

Materials. *N*,*N*-Dimethylformamide (DMF), polyacrylonitrile (PAN, M_w = 150 000), thioacetamide (TAA), sodium molybdate dehydrate (Na_2MoO_4), and MoS_2 powder (<2μm) were purchased from Sigma-Aldrich (USA) and used as received. Electrolyte ($LiPF_6$ in a mixture of ethylene carbonate (EC) and dimethyl carbonate (DMC) at a 1:1 volume ratio, 1 M) and lithium foil were purchased from Charslton Technologies Pte Ltd (Singapore).

Preparation of Hybrid Nanofibers. The MoS_2 was synthesized using a hydrothermal method. Typically, 250 mg of Na_2MoO_4 and 200 mg of TAA were dissolved in 60 mL of deionized (DI) H_2O. The mixture was then transferred to a 100 mL Teflon-lined autoclave and kept at 200 °C for 16 h. After cooling down, the black precipitates were collected and washed with DI water and ethanol for three times. The MoS_2/PAN hybrid nanofibers were then fabricated via conventional single-spinneret electrospinning. First, 150, 300, and 900 mg of MoS_2 was dispersed in 4.4 g of DMF using ultrasonication (Sonic, VCX 750), respectively. A 300 mg portion of PAN was then dissolved into each of the above suspensions through vigorous stirring at 60 °C for about 6 h. The weight ratio of MoS_2 to PAN was 0.5/1, 1/1, and 3/1, respectively. The electrospinning of the suspensions was carried out under a working voltage of 9.5−12.5 kV. The flow rate and needle tip-to-plate collector distance were fixed to 0.3 mL/h and 15 cm, respectively. The as-spun nanofibers were heated from room temperature to 280 °C at a heating rate of 1 °C/min and then stabilized at 280 °C for 1 h in air. After that, the nanofibers were further heated to 700 °C in argon (flow rate: 100 sccm) at a heating rate of 5 °C/min, followed by carbonizing at 700 °C for 3 h. For comparison, neat carbon nanofiber mats were also prepared from PAN by electrospinning, followed by stabilization and carbonization.

Characterization. The morphologies of the hybrid nanofibers were studied using a field emission scanning electron microscope (FESEM, JEOL JSM 7600) at an accelerating voltage of 5 kV and a transmission electron microscope (TEM, JEOL 2100) at 200 kV. The structures of hybrid nanofibers were investigated using an X-ray powder diffractometer (XRD, Bruker D8 Discover) with Cu Kα radiation. The scan rate was 1°/min with a step of 0.02°. The compositions of the hybrid nanofibers were determined by thermogravimetric analysis (TGA, TA Q500). All the samples were heated at a rate of 10 °C/min from room temperature to 600 °C in air.

Electrochemical Measurements. The free-standing MoS_2/C nanofibrous mats and neat carbon mats were used as anodes directly. Lithium foil with a diameter of 14 mm and a thickness of 0.4 mm was used as the counter and reference electrodes. $LiPF_6$ (1 M) in a mixture of EC and DMC (1/1 in v/v) was used as the electrolyte. A half-battery cell was assembled into a 2032 type coin cell in an argon-filled glovebox (MBRAUN UNIlab Pro) using a Celgard 2325 membrane as the separator. The typical loading of the anodes in the electrode was 1−5 mg. The electrochemical tests were performed on a NEWARE BTS-5 V10 mA battery tester at room temperature. The cells were cycled between 0.005 and 3.0 V vs Li^+/Li at 50 mA g^{-1} unless otherwise specified. The cyclic voltammetry (CV) was studied on a PGSTAT302N Autolab electrochemical workstation with a voltage window of 0.005−3.0 V and a scan rate of 0.1 mV/s. The electrochemical impedance spectroscopy (EIS) was measured in the frequency range of 10^{-2} to 10^6 Hz with an AC voltage amplitude of 5 mV. For comparison purposes, electrodes were also prepared through casting a slurry of 80 wt % MoS_2 nanoflakes or commercial MoS_2 powder, 10 wt % super P carbon black, and 10 wt % poly(vinylidene fluoride) in *N*-methyl-2-pyrrolidinone onto a copper foil and investigated.

RESULTS AND DISCUSSION

Structural and Morphological Evolution. The fabrication process for the MoS_2/C nanofibrous mats is illustrated in Figure 1. Thin MoS_2 nanoflakes were first hydrothermally

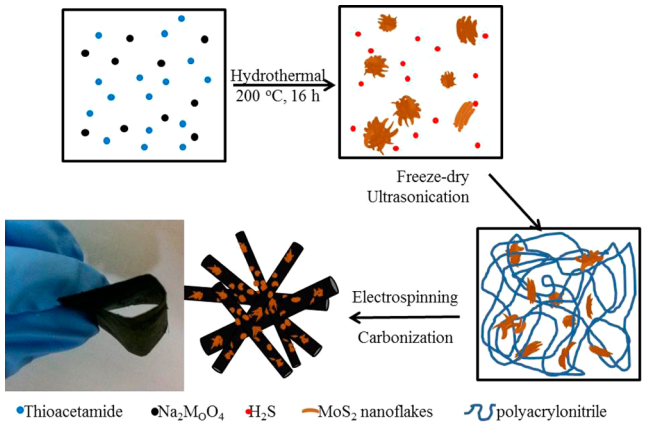

Figure 1. Schematics showing the fabrication process for the highly flexible free-standing MoS_2/C nanofibrous mats. The sample in the picture contains 47% MoS_2.

synthesized from TAA and Na_2MoO_4. TAA, which acts as a sulfurization reagent, decomposes and generates H_2S easily at temperatures above 150 °C through the following reaction: $CH_3CSNH_2 + H_2O \rightarrow CH_3COONH_4 + H_2S$. Mo(VI) is subsequently reduced in solution by H_2S: $Na_2MoO_4 + H_2S \rightarrow MoS_2 + Na_2SO_4 + H_2O + NaOH$. The as-prepared MoS_2 was

then encapsulated in PAN nanofibers via electrospinning. After carbonization, highly flexible free-standing MoS_2/C nanofibrous mats were obtained (Figure 1). Electrospinning-derived neat carbon nanofibers are, in general, fairly brittle,[37] whereas the MoS_2/C hybrid mats are very flexible, as demonstrated in the picture in Figure 1. This may be ascribed to the presence of a high content of thin MoS_2 nanoflakes in the carbon matrix, resulting in thin carbon sections separated by flexible MoS_2 nanoflakes in some regions that may facilitate bending. Indeed, the flexibility of the mat increases with the MoS_2 content. The great difference in flexibility between the MoS_2/C-95 hybrid mat, which has the highest MoS_2 content among all the hybrid mats, and the neat carbon nanofiber mat was demonstrated through repeated bending tests (Figure S1, Supporting Information).

To verify the morphologies of the nanoflakes and nanofibers, TEM and SEM studies were conducted. Figure 2a shows the

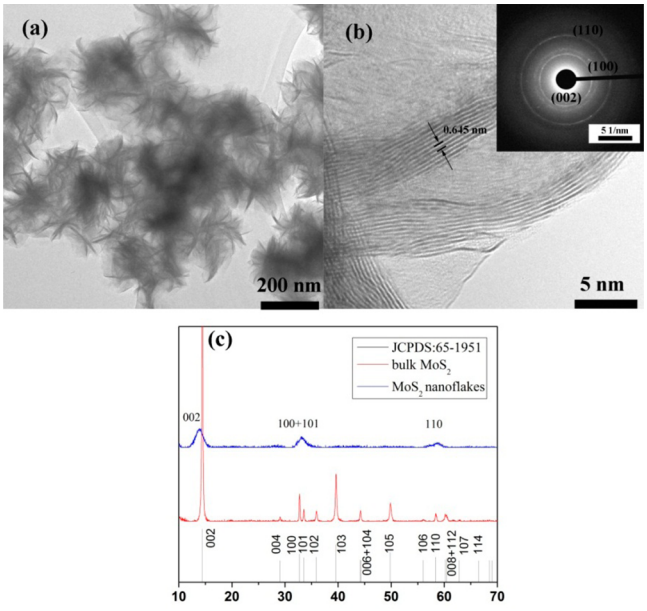

Figure 2. (a, b) TEM images and (c) XRD patterns of the hydrothermally synthesized MoS_2 nanoflakes; the inset in (b) shows the corresponding SAED pattern.

TEM image of the as-synthesized MoS_2 nanoflakes. The nanoflakes are loosely packed, forming a flower-like geometry with a diameter of about 250 nm (Figure 2a). A magnified TEM image in Figure 2b shows that the petal of the "flower" is composed of randomly oriented MoS_2 nanoflakes with a thickness of around 5 nm. This indicates that the number of MoS_2 layers in each nanoflake is less than 10 in most cases. The electron diffraction (SAED) pattern of the MoS_2 nanoflakes (inset of Figure 2b) consists of three diffraction rings that can be indexed to (002), (100), and (110) planes of MoS_2. This is consistent with XRD results (Figure 2c), where three distinct peaks at 2θ = 13.8, 33.1, and 58.5° corresponding to (002), (100), and (110) planes of MoS_2, respectively, are observed.[13,19,28] The XRD pattern of the hydrothermally synthesized MoS_2 is different from that of the bulk MoS_2 power sample and the standard powder diffraction card probably because, under the hydrothermal conditions, the MoS_2 preferentially grows in certain directions and has a relatively low crystallinity and disordered structure. In particular, it is worth noting that the (002) diffraction peak of the nanoflakes (2θ = 13.8°; d = 0.64 nm) is at a lower angle than that of the commercial MoS_2 powder (2θ = 14.4°; d = 0.615 nm), indicating that the interlayer distance of the nanoflakes is expanded. It has been reported that, with 1 mol of lithium intercalation, the c parameter of MoS_2 undergoes an increment of 0.25 Å.[38] The expanded interlayer d spacing would relieve the strain caused by electrochemical lithiation/delithiation during cycling and provide more space for Li ion intercalation with reduced diffusion barriers.[30] In addition, the broad (002) peak suggests that the average crystallite size of the nanoflakes is around 5 nm in the thickness direction. This corresponds to 7−8 MoS_2 layers and is consistent with the TEM result shown above.

Electrospinning was used to fabricate MoS_2/PAN hybrid nanofibers. Upon carbonization, PAN is converted to amorphous carbon while MoS_2 nanoflakes would remain. This is confirmed by XRD results (Figure S2, patterns (a)−(c), Supporting Information). Compared with the as-synthesized MoS_2 nanoflakes, there is no change in the diffraction peak positions after the electrospinning and carbonization, indicating that the incorporation of PAN and the heat treatment do not affect the microstructure of the MoS_2 nanoflakes. The compositions of the MoS_2/C nanofibers were estimated by TGA (Figure S3, Supporting Information). There is a large weight loss in the range of 300−500 °C, which is caused by the combustion of the amorphous carbon and a conversion of MoS_2 to MoO_3 in air. On the basis of the TGA results, the mass fractions of MoS_2 in the hybrid samples are 47, 73, and 95 wt %, respectively, for the samples with feed MoS_2/PAN weight ratios of 0.5/1, 1/1, and 3/1. In the following discussion, the three samples are denoted as MoS_2/C-47, MoS_2/C-73, and MoS_2/C-95, respectively, where the numbers indicate the mass fractions of MoS_2 in the hybrids.

SEM images of the as-spun (left) and carbonized (middle) hybrid nanofibers are shown in Figure 3. The as-spun nanofibers exhibit a "bead-on-string" morphology due to the incorporation of MoS_2 nanoflakes. The average diameters of the as-spun nanofibers increase from 250 nm to nearly 1 μm with the increase of MoS_2 content. For the nanofibers with relatively low MoS_2 contents, the diameters are uniform with

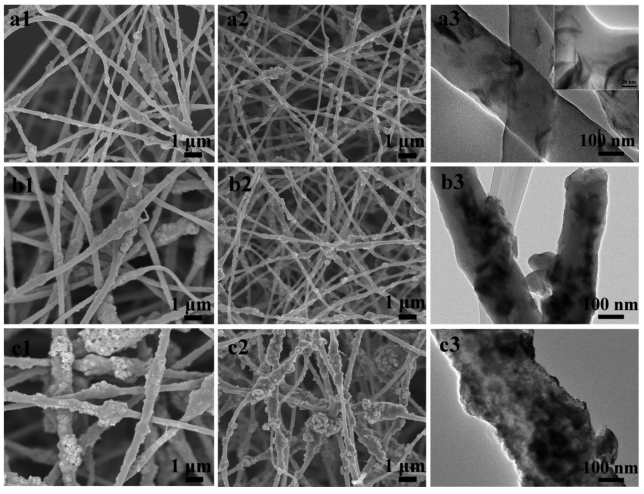

Figure 3. SEM (left, as-spun; middle, carbonized) and TEM (right) images of the hybrid nanofibers. The final MoS_2 contents for (a)−(c) are 47, 73, and 95 wt %, respectively.

dx.doi.org/10.1021/am4058088 | ACS Appl. Mater. Interfaces 2014, 6, 6392−6398

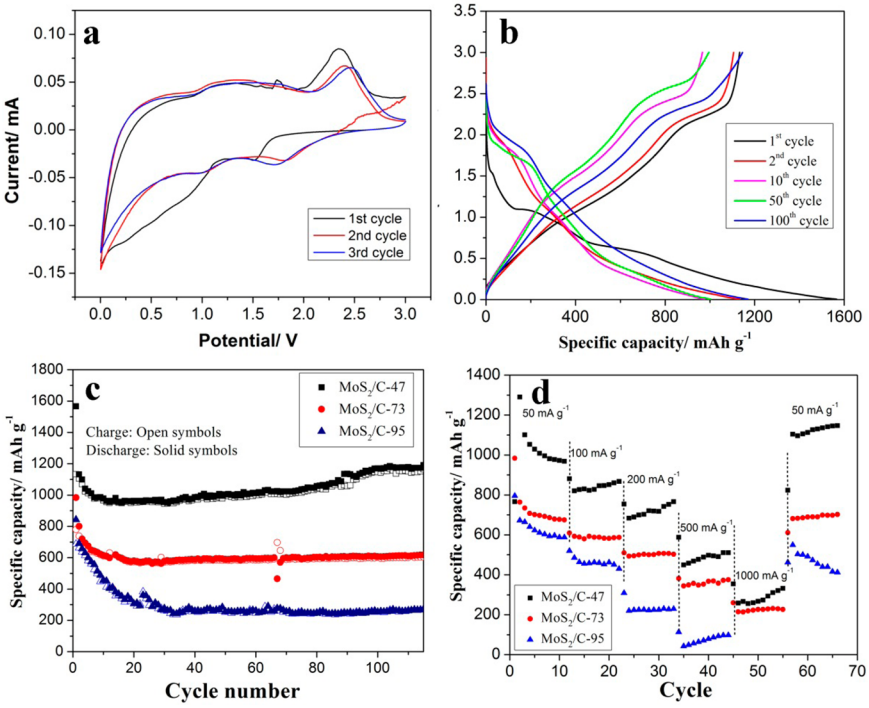

Figure 4. (a) Cyclic voltammograms of MoS_2/C-47 between 0.005 and 3.0 V at a scan rate of 0.1 mV/s. (b) Discharge−charge profiles of MoS_2/C-47 for the 1st, 2nd, 10th, 50th, and 100th cycles. (c) Cycling performances of MoS_2/C-47, MoS_2/C-73, and MoS_2/C-95 at a current density of 50 mA/g. (d) Rate capabilities of the three samples.

only some sparsely distributed beads (Figure $3a_1$,b_1). Differently, for the ones with the highest content of MoS_2, the beads are densely distributed and much larger (Figure $3c_1$), indicating a much severer aggregation of MoS_2 nanoflakes. In addition, some nanoflakes can be found on the surface of the nanofibers. After carbonization, the "bead-on-string" morphology becomes more distinct due to the shrinkage of the nanofibers caused by conversion of PAN to carbon (Figure $3a_2$−c_2). The distribution of the nanoflakes in the carbonized nanofibers was further examined using TEM. As shown in Figure $3a_3$, for MoS_2/C-47, all the MoS_2 nanoflakes are embedded in the carbonized nanofibers and the loosely packed morphology of the nanoflakes are retained. However, at higher MoS_2 contents, especially in MoS_2/C-95, severe aggregation of MoS_2 nanoflakes occurs and some nanoflakes are only partially embedded in the nanofibers (Figure $3c_3$), which may lack conductive and buffering support from the carbon matrix.

Electrochemical Properties. To investigate the performance of the MoS_2/C nanofibrous mat as an LIB anode, first, the lithiation/delithiation behaviors were examined via cyclic voltammetry (CV), taking MoS_2/C-47 as an example (Figure 4a). The reduction peak at 1.6 V in the first cathodic curve is assigned to the reduction of PAN-derived oxygen/nitrogen-containing amorphous carbon.[39] The slope at about 1.1 V is indicative of the formation of Li_xMoS_2, which then decomposes into Mo nanoparticles embedded in Li_2S, giving a cathodic peak at about 0.5 V. This two-step discharge process can be expressed by the following two reaction equations:[27]

$$MoS_2 + xLi^+ + xe^- = Li_xMoS_2 \quad (1)$$

$$Li_xMoS_2 + 4Li^+ + 4e^- = 2Li_2S + Mo/Li_x \quad (2)$$

The inconspicuous conversion in the first discharge of MoS_2/C-47 is caused by low crystallinity and defect sites/disordered structure of the graphene-like MoS_2 as well as the contribution of amorphous carbon (Figure S4, Supporting Information).[20,24] The slope below 0.3 V is assigned to the formation of a solid electrolyte interphase (SEI) film. During the anodic scanning, Li^+ stored within the amorphous carbon and defects of MoS_2 are first released, leading to a broad oxidation peak centered at 1.2 V. Two pronounced peaks at 1.7 and 2.3 V are associated with the delithiation of Mo and the oxidation of Li_2S to sulfur, respectively. Therefore, MoS_2 converts to a mixture of sulfur and Mo metal after the first cycle.[27] Accordingly, in the following cycles, the reduction peak at 2.0 V can be attributed to the formation of Li_2S, and the association of Li^+ ions with Mo is found at 1.0 V.

Figure 4c shows the cycling performance of the MoS_2/C nanofibers with varied MoS_2 contents. The capacity is normalized to the mass of MoS_2 by taking the capacity of amorphous carbon as that of graphite, 372 mAh/g. It is shown that the cycling performance of MoS_2/C nanofibers is much better than that of the anodes based on the MoS_2 powder and MoS_2 nanoflakes (Figure S5, Supporting Information). This is ascribed to the expanded interlayer *d* spacing of the MoS_2 nanoflakes than that of the MoS_2 powder, as well as the fibrous morphology induced by electrospinning. On one hand, the larger interlayer distance of nanoflakes relaxes the stress, lowers the energy barrier, and provides more defects for Li^+ ion intercalation. The small thickness of MoS_2 nanoflakes shortens the electron and Li^+ ion pathway.[40] On the other hand, the carbon matrix stabilizes the disordered structure of MoS_2, tolerates local volume expansion/contraction during repetitive lithium storage/release, and avoids the loss of polysulfide intermediates.[41−44] Furthermore, the conductivity of the whole anode is also greatly enhanced. The electrospun nanofibers, typically meters in length, need only a few interfiber contacts to

dx.doi.org/10.1021/am4058088 | ACS Appl. Mater. Interfaces 2014, 6, 6392−6398

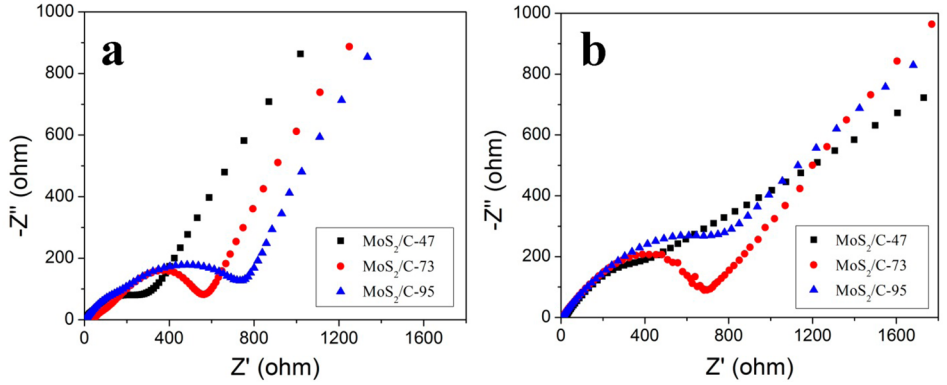

Figure 5. Nyquist plots of MoS_2/C-47, MoS_2/C-73, and MoS_2/C-95 measured at OCPs (a) before and (b) after cycles.

achieve sufficient electron transport, which is very important for the hybrid owing to the semiconducting nature of MoS_2.

The initial charge capacity of MoS_2/C-47 is 1133 mAh/g with a Coulombic efficiency of 73% (Figure 4b). The irreversible capacity loss is mainly caused by the formation of the SEI film in the initial cycle. In the following cycles, the Coulombic efficiency remains at almost 100% with an excellent cycling performance achieved. From 20 cycles onwards, the specific capacity of MoS_2/C-47 increases continuously and reaches 1150 mAh/g at the 100th cycle, which may be attributed to the activation of the Li^+ ion pathway between the electrolyte and electrode during cycling.[31] The stable cycling performance shows superiority over other MoS_2-based anodes,[14,29,30] indicating that the carbon matrix not only enhances the electrical conductivity of the electrode but also confines the active material within the matrix, alleviating the shuttle effect of soluble polysulfides.[45,46] Although MoS_2/C-73 has a much higher MoS_2 content than MoS_2/C-47, the initial charge capacity and reversible capacity of MoS_2/C-73 are significantly lower than that of MoS_2/C-47. With the extremely high MoS_2 content, MoS_2/C-95 suffers more severe capacity loss upon cycling, from an initial capacity of 687 mAh/g to 260 mAh/g at the 30th cycle. The fast capacity decay of MoS_2/C-73 and MoS_2/C-95 can be attributed to detachment of the MoS_2 nanoflakes from the carbon nanofibers. More evidence for this will be shown later.

The electrochemical performances of neat carbon mats derived from electrospun PAN are shown in Figure S4 (Supporting Information). The neat carbon mats could deliver a reversible capacity of 310 mAh/g at the 50th cycle, close to the theoretical capacity of graphite. It is reported that some N-rich amorphous carbon could store over 1500 mAh/g at low and intermediate rates.[47−51] For PAN-based carbon fiber mats, however, capacities of less than 400 mAh/g are usually observed probably because of their nonporous fibrous morphology.[52,53]

The rate capabilities of the MoS_2/C nanofibers are shown in Figure 4d. Beneficial from the good dispersion of MoS_2 in the carbon matrix, MoS_2/C-47 exhibits the best rate performance among the three samples. Even at a high rate of 1000 mA/g, a discharge capacity of 250−350 mAh/g can still be achieved. The reversible capacity restores to 1100 mAh/g when the current rate is changed back to 50 mA/g, and the capacity keeps ascending during subsequent cycling, approaching its initial capacity. On the contrary, the other two samples exhibit poor rate performance. MoS_2/C-95, for instance, only delivers a capacity of about 100 mAh/g at a current density of 500 mA/g and suffers a significant capacity loss when the current rate is reset to 50 mA/g.

To verify the mechanism for the significant effect of MoS_2 content on electrochemical performance of the hybrid nanofibrous mats, AC impedance studies were carried out to analyze the charge-transfer resistance across MoS_2/C-47, MoS_2/C-73, and MoS_2/C-95 electrodes at open cycle potentials (OCPs) before and after cycling. The Nyquist plots obtained are shown in Figure 5. All the plots consist of two semicircles at high and medium frequencies and a straight line inclined at a constant angle at low frequencies, corresponding to the resistance of the SEI film, charge-transfer resistance at the electrolyte/electrode interface, and the solid-state diffusion resistance of Li^+ in the electrode, respectively.[40] With the increase of MoS_2 content, the charge-transfer resistance increases significantly, verifying that the aggregation of nanoflakes at high MoS_2 contents indeed hinders electron and ion transport. Compared with Figure S4d (Supporting Information), the incorporation of MoS_2 increases the charge-transfer resistance of the electrodes due to the semiconductive nature of MoS_2. After the cycling test, the interfacial charge-transfer resistance of the electrodes is higher than that before the cycling for all samples owing to the insulating SEI layer formed and the destruction of the MoS_2 structure during cycling. Nevertheless, MoS_2/C-47 still exhibits the lowest charge-transfer resistance, suggesting the smoothest diffusion for lithium ions and electrons, and hence justifying its highest cycle capacity.

To further study the mechanism for the strong dependence of cycle capacity on MoS_2 content, the morphologies of MoS_2/C-47 and MoS_2/C-95 were examined after the cycling test. Before the examination, the electrodes were washed with ethanol for three times to eliminate the residues. The SEM and TEM images in Figure 6a1,a2 show that the morphology of MoS_2/C-47 is intact after cycling, indicating effective confinement of active materials by the carbon matrix and thus excellent structure stability. By contrast, the surface of MoS_2/C-95 becomes smoother with lesser aggregated MoS_2 on the surface after cycling, although the nanofibrous morphology remains (Figure 6b1,b2). Some partially embedded MoS_2 nanoflakes are peeled off from the carbon nanofibers because the carbon matrix is unable to anchor the expanded nanoflakes during cycling, leaving some large cavities on the nanofiber surface (Figure 6b3,b4). Such detachment induces severe capacity fading. Indeed, better electrochemical performance can be achieved by introducing a very thin carbon coating onto the surface of MoS_2/C-95 nanofibers (Figures S6−S8, Supporting

dx.doi.org/10.1021/am4058088 | ACS Appl. Mater. Interfaces 2014, 6, 6392−6398

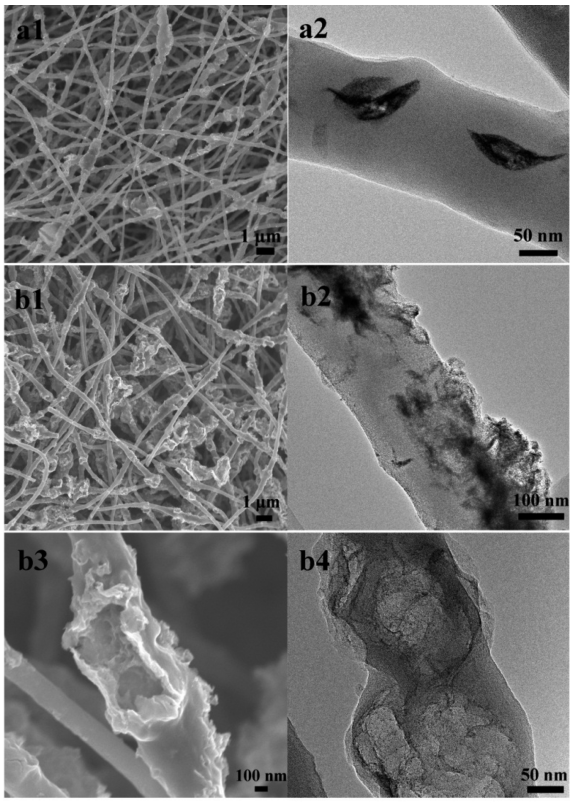

Figure 6. SEM (left) and TEM (right) images of (a) MoS_2/C-47 and (b) MoS_2/C-95 after the cycling test.

Information). In this case, the carbon coating effectively prevents the detachment of MoS_2 nanoflakes since they are well-protected by carbon.

CONCLUSIONS

In this work, flexible and free-standing MoS_2/C hybrid nanofibrous mats were fabricated by electrospinning, followed by carbonization, for the first time, and their excellent performance as anode materials for lithium-ion batteries was demonstrated. Among the three MoS_2/C hybrids, MoS_2/C-47 shows the best electrochemical properties with a stable capacity of 1000−1200 mAh/g and a reversible capacity of ∼350 mAh/g at a high current density of 1000 mA/g. The expansion of the interlayer *d* spacing of MoS_2 nanoflakes, the effective confinement of the active material by the carbon matrix, the good electron transport provided by the high aspect ratio of the electrospinning-derived carbon nanofibers, and the robustness of the hybrid nanofibrous structure are believed to be the main reasons for the high specific capacity, excellent cycling, and rate stability achieved. The approach enables large-scale preparation of high-performance MoS_2 electrodes and also provides a general strategy to immobilize soluble polysulfide intermediates in lithium−sulfur batteries. The highly flexible mats may also facilitate flexible LIBs.

ASSOCIATED CONTENT

Supporting Information

Figures showing repeated bending tests, XRD patterns, TGA curves, electrochemical performances, cycling performances, morphologies and electrochemical characterization, and Nyquist plot and movies showing bending tests. This material is available free of charge via the Internet at http://pubs.acs.org.

AUTHOR INFORMATION

Corresponding Author

*E-mail: ASXHLu@ntu.edu.sg.

Notes

The authors declare no competing financial interest.

REFERENCES

(1) Cavaliere, S.; Subianto, S.; Savych, I.; Jones, D. J.; Rozière, J. Electrospinning: Designed Architectures for Energy Conversion and Storage Devices. *Energy Environ. Sci.* **2011**, *4*, 4761−4785.
(2) Service, R. F. Getting There. *Science* **2011**, *332*, 1494−1496.
(3) Heising, J.; Kanatzidis, M. G. Exfoliated and Restacked MoS_2 and WS_2: Ionic or Neutral Species? Encapsulation and Ordering of Hard Electropositive Cations. *J. Am. Chem. Soc.* **1999**, *121*, 11720−11732.
(4) Ramakrishna Matte, H. S. S.; Gomathi, A.; Manna, A. K.; Late, D. J.; Datta, R.; Pati, S. K.; Rao, C. N. R. MoS_2 and WS_2 Analogues of Graphene. *Angew. Chem., Int. Ed.* **2010**, *49*, 4059−4062.
(5) Rao, C. N. R.; Nag, A. Inorganic Analogues of Graphene. *Eur. J. Inorg. Chem.* **2010**, 4244−4250.
(6) Geim, A. K.; Novoselov, K. S. The Rise of Graphene. *Nat. Mater.* **2007**, *6*, 183−191.
(7) Li, Y.; Wang, H.; Xie, L.; Liang, Y.; Hong, G.; Dai, H. MoS_2 Nanoparticles Grown on Graphene: An Advanced Catalyst for the Hydrogen Evolution Reaction. *J. Am. Chem. Soc.* **2011**, *133*, 7296−7299.
(8) Xiang, Q.; Yu, J.; Jaroniec, M. Synergetic Effect of MoS_2 and Graphene as Cocatalysts for Enhanced Photocatalytic H_2 Production Activity of TiO_2 Nanoparticles. *J. Am. Chem. Soc.* **2012**, *134*, 6575−6578.
(9) Soon, J. M.; Loh, K. P. Electrochemical Double-Layer Capacitance of MoS_2 Nanowall Films. *Electrochem. Solid-State Lett.* **2007**, *10*, A250−A254.
(10) Sun, M.; Adjaye, J.; Nelson, A. E. Theoretical Investigations of the Structures and Properties of Molybdenum-Based Sulfide Catalysts. *Appl. Catal., A* **2004**, *263*, 131−143.
(11) Chhowalla, M.; Amaratunga, G. A. Thin Films of Fullerene-Like MoS_2 Nanoparticles with Ultra-Low Friction and Wear. *Nature* **2000**, *407*, 164−167.
(12) Zhang, C.; Wang, Z.; Guo, Z.; Lou, X. W. Synthesis of MoS_2−C One-Dimensional Nanostructures with Improved Lithium Storage Properties. *ACS Appl. Mater. Interfaces* **2012**, *4*, 3765−3768.
(13) Li, H.; Li, W.; Ma, L.; Chen, W.; Wang, J. Electrochemical Lithiation/Delithiation Performances of 3D Flowerlike MoS_2 Powders Prepared by Ionic Liquid Assisted Hydrothermal Route. *J. Alloys Compd.* **2009**, *471*, 442−447.
(14) Ding, S.; Chen, J. S.; Lou, X. W. Glucose-Assisted Growth of MoS_2 Nanosheets on CNT Backbone for Improved Lithium Storage Properties. *Chem.—Eur. J.* **2011**, *17*, 13142−13145.
(15) Feng, C.; Ma, J.; Li, H.; Zeng, R.; Guo, Z.; Liu, H. Synthesis of Molybdenum Disulfide (MoS_2) for Lithium Ion Battery Applications. *Mater. Res. Bull.* **2009**, *44*, 1811−1815.
(16) Miki, Y.; Nakazato, D.; Ikuta, H.; Uchida, T.; Wakihara, M. Amorphous MoS_2 as the Cathode of Lithium Secondary Batteries. *J. Power Sources* **1995**, *54*, 508−510.
(17) Julien, C.; Saikh, S.; Nazri, G. Electrochemical Studies of Disordered MoS_2 as Cathode Material in Lithium Batteries. *Mater. Sci. Eng., B* **1992**, *15*, 73−77.
(18) Sen, U. K.; Mitra, S. High-Rate and High-Energy-Density Lithium-Ion Battery Anode Containing 2D MoS_2 Nanowall and Cellulose Binder. *ACS Appl. Mater. Interfaces* **2013**, *5*, 1240−1247.
(19) Wang, M.; Li, G.; Xu, H.; Qian, Y.; Yang, J. Enhanced Lithium Storage Performances of Hierarchical Hollow MoS_2 Nanoparticles Assembled from Nanosheets. *ACS Appl. Mater. Interfaces* **2013**, *5*, 1003−1008.
(20) Wang, Z.; Chen, T.; Chen, W.; Chang, K.; Ma, L.; Huang, G.; Chen, D.; Lee, J. Y. CTAB-Assisted Synthesis of Single-Layer MoS_2-Graphene Composites as Anode Materials of Li-Ion Batteries. *J. Mater. Chem. A* **2013**, *1*, 2202−2210.

(21) Bindumadhavan, K.; Srivastava, S. K.; Mahanty, S. MoS_2–MWCNT Hybrids as a Superior Anode in Lithium-Ion Batteries. *Chem. Commun.* **2013**, *49*, 1823–1825.
(22) Park, S.-K.; Yu, S.-H.; Woo, S.; Quan, B.; Lee, D.-C.; Kim, M. K.; Sung, Y.-E.; Piao, Y. A Simple L-Cysteine-Assisted Method for the Growth of MoS_2 Nanosheets on Carbon Nanotubes for High-Performance Lithium Ion Batteries. *Dalton Trans.* **2013**, *42*, 2399–2405.
(23) Chang, K.; Chen, W. L-Cysteine-Assisted Synthesis of Layered MoS_2/Graphene Composites with Excellent Electrochemical Performances for Lithium Ion Batteries. *ACS Nano* **2011**, *5*, 4720–4728.
(24) Chang, K.; Chen, W. Single-Layer MoS_2/Graphene Dispersed in Amorphous Carbon: Towards High Electrochemical Performances in Rechargeable Lithium Ion Batteries. *J. Mater. Chem.* **2011**, *21*, 17175–17184.
(25) Chang, K.; Chen, W.; Ma, L.; Li, H.; Li, H.; Huang, F.; Xu, Z.; Zhang, Q.; Lee, J.-Y. Graphene-like MoS_2/Amorphous Carbon Composites with High Capacity and Excellent Stability as Anode Materials for Lithium Ion Batteries. *J. Mater. Chem.* **2011**, *21*, 6251–6257.
(26) Xiao, J.; Choi, D.; Cosimbescu, L.; Koech, P.; Liu, J.; Lemmon, J. P. Exfoliated MoS_2 Nanocomposite as an Anode Material for Lithium Ion Batteries. *Chem. Mater.* **2010**, *22*, 4522–4524.
(27) Xiao, J.; Wang, X.; Yang, X.-Q.; Xun, S.; Liu, G.; Koech, P. K.; Liu, J.; Lemmon, J. P. Electrochemically Induced High Capacity Displacement Reaction of PEO/MoS_2/Graphene Nanocomposites with Lithium. *Adv. Funct. Mater.* **2011**, *21*, 2840–2846.
(28) Xie, J.; Zhang, H.; Li, S.; Wang, R.; Sun, X.; Zhou, M.; Zhou, J.; Lou, X. W. D.; Xie, Y. Defect-Rich MoS_2 Ultrathin Nanosheets with Additional Active Edge Sites for Enhanced Electrocatalytic Hydrogen Evolution. *Adv. Mater.* **2013**, *25*, 5807–5813.
(29) Fang, X.; Yu, X.; Liao, S.; Shi, Y.; Hu, Y.-S.; Wang, Z.; Stucky, G. D.; Chen, L. Lithium Storage Performance in Ordered Mesoporous MoS_2 Electrode Material. *Microporous Mesoporous Mater.* **2012**, *151*, 418–423.
(30) Du, G.; Guo, Z.; Wang, S.; Zeng, R.; Chen, Z.; Liu, H. Superior Stability and High Capacity of Restacked Molybdenum Disulfide as Anode Material for Lithium Ion Batteries. *Chem. Commun.* **2010**, *46*, 1106–1108.
(31) Hwang, H.; Kim, H.; Cho, J. MoS_2 Nanoplates Consisting of Disordered Graphene-like Layers for High Rate Lithium Battery Anode Materials. *Nano Lett.* **2011**, *11*, 4826–4830.
(32) Kong, J.; Wong, S. Y.; Zhang, Y.; Tan, H. R.; Li, X.; Lu, X. One-Dimensional Carbon–SnO_2 and SnO_2 Nanostructures Via Single-Spinneret Electrospinning: Tunable Morphology and the Underlying Mechanism. *J. Mater. Chem.* **2011**, *21*, 15928–15934.
(33) Ji, L.; Lin, Z.; Guo, B.; Medford, A. J.; Zhang, X. Assembly of Carbon–SnO_2 Core–Sheath Composite Nanofibers for Superior Lithium Storage. *Chem.—Eur. J.* **2010**, *16*, 11543–11548.
(34) Ji, L.; Jung, K.-H.; Medford, A. J.; Zhang, X. Electrospun Polyacrylonitrile Fibers with Dispersed Si Nanoparticles and Their Electrochemical Behaviors after Carbonization. *J. Mater. Chem.* **2009**, *19*, 4992–4997.
(35) Ji, L.; Zhang, X. Evaluation of Si/Carbon Composite Nanofiber-Based Insertion Anodes for New-Generation Rechargeable Lithium-Ion Batteries. *Energy Environ. Sci.* **2010**, *3*, 124–129.
(36) Tarascon, J.-M.; Armand, M. Issues and Challenges Facing Rechargeable Lithium Batteries. *Nature* **2001**, *414*, 359–367.
(37) Zussman, E.; Chen, X.; Ding, W.; Calabri, L.; Dikin, D.; Quintana, J.; Ruoff, R. Mechanical and Structural Characterization of Electrospun PAN-Derived Carbon Nanofibers. *Carbon* **2005**, *43*, 2175–2185.
(38) Santa-Ana, M. A.; Sanchez, V.; Gonzalez, G. Temperature Effects on the Diffusion of Lithium in MoS_2. *Electrochim. Acta* **1995**, *40*, 1773–1775.
(39) Huang, G.; Chen, T.; Chen, W.; Wang, Z.; Chang, K.; Ma, L.; Huang, F.; Chen, D.; Lee, J. Y. Graphene-like MoS_2/Graphene Composites: Cationic Surfactant-Assisted Hydrothermal Synthesis and Electrochemical Reversible Storage of Lithium. *Small* **2013**, *9*, 3693–3703.
(40) Wang, Q.; Li, J. Facilitated Lithium Storage in MoS_2 Overlayers Supported on Coaxial Carbon Nanotubes. *J. Phys. Chem. C* **2007**, *111*, 1675–1682.
(41) Gao, M.-R.; Xu, Y.-F.; Jiang, J.; Yu, S.-H. Nanostructured Metal Chalcogenides: Synthesis, Modification, and Applications in Energy Conversion and Storage Devices. *Chem. Soc. Rev.* **2013**, *42*, 2986–3017.
(42) Huang, X.; Zeng, Z.; Zhang, H. Metal Dichalcogenide Nanosheets: Preparation, Properties and Applications. *Chem. Soc. Rev.* **2013**, *42*, 1934–1946.
(43) Stephenson, T.; Li, Z.; Olsen, B.; Mitlin, D. Lithium Ion Battery Applications of Molybdenum Disulfide (MoS_2) Nanocomposites. *Energy Environ. Sci.* **2014**, *7*, 209–231.
(44) Lai, C.-H.; Lu, M.-Y.; Chen, L.-J. Metal Sulfide Nanostructures: Synthesis, Properties and Applications in Energy Conversion and Storage. *J. Mater. Chem.* **2012**, *22*, 19–30.
(45) Ji, X.; Lee, K. T.; Nazar, L. F. A Highly Ordered Nanostructured Carbon–Sulphur Cathode for Lithium–Sulphur Batteries. *Nat. Mater.* **2009**, *8*, 500–506.
(46) Li, D.; Han, F.; Wang, S.; Cheng, F.; Sun, Q.; Li, W.-C. High Sulfur Loading Cathodes Fabricated Using Peapodlike, Large Pore Volume Mesoporous Carbon for Lithium–Sulfur Battery. *ACS Appl. Mater. Interfaces* **2013**, *5*, 2208–2213.
(47) Zhao, L.; Fan, L.-Z.; Zhou, M.-Q.; Guan, H.; Qiao, S.; Antonietti, M.; Titirici, M.-M. Nitrogen-Containing Hydrothermal Carbons with Superior Performance in Supercapacitors. *Adv. Mater.* **2010**, *22*, 5202–5206.
(48) Li, Z.; Xu, Z.; Tan, X.; Wang, H.; Holt, C. M. B.; Stephenson, T.; Olsen, B. C.; Mitlin, D. Mesoporous Nitrogen-Rich Carbons Derived from Protein for Ultra-High Capacity Battery Anodes and Supercapacitors. *Energy Environ. Sci.* **2013**, *6*, 871–878.
(49) Raymundo-Piñero, E.; Cadek, M.; Béguin, F. Tuning Carbon Materials for Supercapacitors by Direct Pyrolysis of Seaweeds. *Adv. Funct. Mater.* **2009**, *19*, 1032–1039.
(50) Aboutalebi, S. H.; Chidembo, A. T.; Salari, M.; Konstantinov, K.; Wexler, D.; Liu, H. K.; Dou, S. X. Comparison of GO, GO/MWCNTs Composite and MWCNTs as Potential Electrode Materials for Supercapacitors. *Energy Environ. Sci.* **2011**, *4*, 1855–1865.
(51) Xu, B.; Yue, S.; Sui, Z.; Zhang, X.; Hou, S.; Cao, G.; Yang, Y. What is the Choice for Supercapacitors: Graphene or Graphene Oxide? *Energy Environ. Sci.* **2011**, *4*, 2826–2830.
(52) Kim, C.; Yang, K. S.; Kojima, M.; Yoshida, K.; Kim, Y. J.; Kim, Y. A.; Endo, M. Fabrication of Electrospinning-Derived Carbon Nanofiber Webs for the Anode Material of Lithium-Ion Secondary Batteries. *Adv. Funct. Mater.* **2006**, *16*, 2393–2397.
(53) Lee, J. K.; An, K. W.; Ju, J. B.; Cho, B. W.; Cho, W. I.; Park, D.; Yun, K. S. Electrochemical Properties of PAN-Based Carbon Fibers as Anodes for Rechargeable Lithium Ion Batteries. *Carbon* **2001**, *39*, 1299–1305.